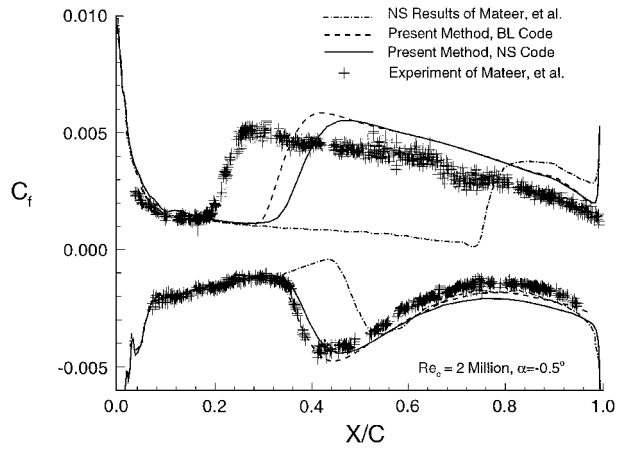

Fig. 2 Comparison of present method and e^n method with the airfoil experiment of Mateer et al.,[13] $Re_c = 2 \times 10^6$, $\alpha = -0.5$ deg.

Conclusion

In summary, the present model requires replacing ν_t and τ_k in any two-equation turbulence code by Eqs. (8) and (9) to calculate transition onset and the complete flowfield. Because of this, the present approach provides an inexpensive alternative to the e^n method and methods based on the nonlinear PSE.

Acknowledgments

This work is supported, in part, by NASA Grant NAG-1-244 from NASA Langley Research Center. Part of the computations were carried out at the North Carolina Supercomputing Center. The authors would like to acknowledge helpful discussions with Ndaona Chokani of North Carolina State University.

References

[1]Mack, L. M., "Transition Prediction and Linear Stability Theory," AGARD CP-224, 1977, pp. 1-1–1-22.

[2]Saric, W. S., "Physical Description of Boundary Layer Transition: Experimental Evidence," AGARD Rept. 793, March 1993.

[3]Herbert, T., "Parabolized Stability Equations," AGARD Rept. 794, March 1993.

[4]Robinson, D. F., Harris, J. E., and Hassan, H. A., "Unified Turbulence Closure Model for Axisymmetric and Planar Free Shear Flows," *AIAA Journal*, Vol. 33, No. 12, 1995, pp. 2325–2331.

[5]Warren, E. S., and Hassan, H. A., "An Alternative to the e^n Method for Determining Onset of Transition," AIAA Paper 97-0825, Jan. 1997.

[6]Robinson, D. F., and Hassan, H. A., "A Two Equation Turbulence Closure Model for Wall Bounded and Free Shear Flows," AIAA Paper 96-2057, June 1996.

[7]Obremski, H. J., Morkovin, M. V., and Landahl, M., "Portfolio of Stability Characteristics of Incompressible Boundary Layers," AGARDograph 134, March 1969.

[8]Walker, G. J., "Transitional Flow on Axial Turbomachine Blading," *AIAA Journal*, Vol. 27, No. 5, 1989, pp. 595–602.

[9]Dhawan, S., and Narasimha, R., "Some Properties of Boundary Layer Flow During Transition from Laminar to Turbulent Motion," *Journal of Fluid Mechanics*, Vol. 3, No. 4, 1958, pp. 418–436.

[10]Schubauer, G. B., and Klebanoff, P. S., "Contributions on the Mechanics of Boundary-Layer Transition," NACA Rept. 1289, 1956.

[11]Schubauer, G. B., and Skramstad, H. K., "Laminar Boundary Layer Oscillations and Transition on a Flat Plate," NACA Rept. 909, 1948.

[12]Harris, J. E., and Blanchard, D. K., "Computer Program for Solving Laminar, Transitional, or Turbulent Compressible Boundary-Layer Equations for Two-Dimensional and Axisymmetric Flow," NASA TM 83207, Feb. 1982.

[13]Mateer, G. G., Monson, D. J., and Menter, F. R., "Skin-Friction Measurements and Calculations on a Lifting Airfoil," *AIAA Journal*, Vol. 34, No. 2, 1996, pp. 231–236.

[14]Menter, F. R., "Two-Equation Eddy-Viscosity Turbulence Models for Engineering Applications," *AIAA Journal*, Vol. 32, No. 8, 1994, pp. 1598–1605.

A. Plotkin
Associate Editor

Shock Pattern of a Triple-Shock Turbulent Interaction

Datta Gaitonde* and J. S. Shang†
U.S. Air Force Wright Laboratory,
Wright–Patterson Air Force Base, Ohio 45433-7913

I. Introduction

An important factor limiting the performance of supersonic aircraft propulsion systems is the phenomenon of three-dimensional separation that occurs in the compression process. The consequent formation of vortical structures reduces pressure recovery and increases distortion. One of the primary indicators of the flowfield is the shock structure. In a recent work, Garrison et al.[1] present planar laser scattering (PLS) images of the shock structure in the triple-shock (TS) interaction shown schematically in Fig. 1. The incoming equilibrium turbulent boundary layer is subjected to shock waves arising at three compression surfaces, viz., the two 15-deg fins and the 10-deg ramp. The flowfield represents a progression in complexity from a single intersecting wedge corner[2] and the double-fin (DF) configurations, e.g., Ref. 3. Rapid advances in computational technology in the past decade have made possible increasingly sophisticated theoretical studies to model such interactions. It is the objective of this work to computationally investigate the complex shock structure arising in the TS interaction. We validate the computed structure by comparison with the PLS observations of Ref. 1. Subsequently, the computations are employed to map the details of the shock intersections. The flowfield parameters are summarized in Fig. 1. For brevity, the reader is referred to Ref. 4 for computational details. The model is similar to that employed successfully for DF shock structure.[3] Briefly, the three-dimensional Reynolds-averaged equations are solved with a high-resolution upwind-biased scheme and a two-equation k–ϵ turbulence model. The mesh employed consists of $99 \times 107 \times 114$ nodes. A discussion of mesh adequacy can be found in Ref. 4.

II. Results

The shock structure of TS is highly three dimensional. To facilitate description and comparison with experiment, we employ spanwise cutting planes of the type shown schematically in Fig. 1. Figure 2 depicts the computed results with the magnitude of the three-dimensional pressure gradient $|\nabla p|$ on a sequence of such planes. In each frame, the left, right, and bottom boundaries are the symmetry plane, the right fin, and the ramp surfaces, respectively. The PLS observations may be found in Ref. 1 and are not reproduced here. We note, however, that the comparison with the present calculations is excellent and the modest discrepancies that do exist are noted later. Further, the nomenclature employed (Fig. 2) is identical to that of Ref. 1 with the exception of feature 18 as discussed later.

The shock systems from the left and right fins cross at the symmetry plane. Thus, as the cutting plane is moved downstream, the shock system appears to reflect off the symmetry plane and is described later in this manner. In the subsequent discussion, no temporal significance is attached to terms denoting movement or to the superposed arrows. They refer rather to the apparent motion of the shock trace as the cutting plane is moved downstream. In this context, shocks generally "move" into the upstream fluid and impart it a velocity in the same direction.

Figure 2a shows the structure at a station where the shock systems originating at each ramp-fin corner have not yet "propagated" to the symmetry plane. The features include the inviscid fin shock (1), the corner shock (2), the ramp shock (3), an "embedded" fin

Received Jan. 24, 1997; revision received Aug. 13, 1997; accepted for publication Sept. 24, 1997. This paper is declared a work of the U.S. Government and is not subject to copyright protection in the United States.

*Visiting Scientist, Ohio Aerospace Institute, FIMC, Building 450, Suite 7, 2645 Fifth Street. Senior Member AIAA.

†Senior Scientist, FIMC, Building 450, Suite 7, 2645 Fifth Street. Fellow AIAA.

shock (4) that is curved, associated fin separation (5) and fin rear (6) shocks, and finally a ramp embedded shock (7) with its associated ramp separation (8) and ramp rear shocks (9). There are four triple-points formed by the intersections of 1-2-7, 2-3-4, 4-5-6, and 7-8-9, respectively. In the notation of Ref. 1, features 10 and 11 denote intersections of the slip surfaces and the separation region, respectively, and are not shown in Fig. 2 because they are not evident in the pressure field. They may be found in the computed density field as shown in Ref. 4.

In Fig. 2b, 5 reflects in an irregular manner from the symmetry plane, resulting in a Mach stem 12 and a reflected fin separation shock 13, which serves to align the fluid previously deflected parallel to the right fin in a direction parallel to the symmetry plane. The curvature of 4 is now more pronounced. The shock 7 moves upward more rapidly than 3 because the former processes fluid downstream of 1, which is at a lower Mach number. For the same reason, 4 approaches the symmetry plane faster than 1. These trends cause a lengthening of the corner shock trace 2.

In Fig. 2c, 13 and 6 have crossed each other. One minor discrepancy with the experimental sketches is in the manner of crossing of 13 and 6. In the computations, this crossing occurs where 5 is terminated and the shocks 6 and 13 coincide as do the two triple points associated with them, 4-5-6 and 5-12-13. In contrast, in the experimental sketch, 13 and 6 cross before the termination of 5.

Figure 2d is located just upstream of where 4 reflects off the symmetry plane. This reflection occurs in an intricate manner, and the dominant aspects are shown in Figs. 2c–2e. Close examination of several variables in the computed field suggests the details shown schematically in Fig. 3. Figure 3a is a schematic of Fig. 2c. In Fig. 3b, 4 moves toward the centerline, and the upper and lower triple points reach the symmetry plane. This eliminates the ramp shock 3 as a separate entity. In Fig. 3c, the distorted segment of 4 between 6 and 13 vanishes, and 4 reflects at its upper and lower extremes to form 15. Because the outer parts reflect first, a pinched appearance is evident. The corner shock 2 reflects in an irregular fashion, with the formation of a Mach stem 12. This process continues in Fig. 3d where, at the lower end of 15, 6 reflects to form 14 in a regular fashion. In Fig. 3e, the reflection of 4 is completed to form 15. A new shock denoted 12a is formed, whereas the region beneath is occupied by a weak expansion (EXP). This 12a-EXP combination has been observed in previous DF computations.[3] The strength of this pair of features diminishes rapidly in the streamwise direction and is associated with the displacement effect of the separated boundary layer underneath.[3] In Fig. 3f, the reflection of 6 is complete. A new duo of slip-surface intersections (which appear as lines on the cutting plane) appears between 15 and the symmetry plane as shown. The reflected shock 15 straightens as it moves toward the fins where the degree of shear diminishes. All of the features in Fig. 3f are visible in Fig. 2e.

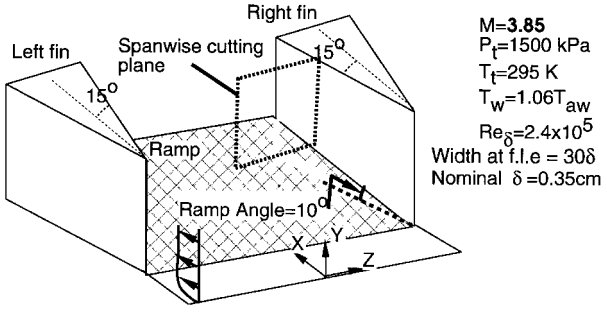

Fig. 1 Schematic of triple-shock interaction configuration and flow parameters.

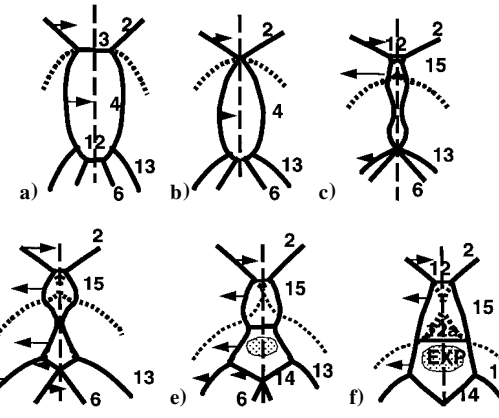

Fig. 3 Schematic representation of reflection of fin-embedded shock 4 from symmetry plane. Not to scale.

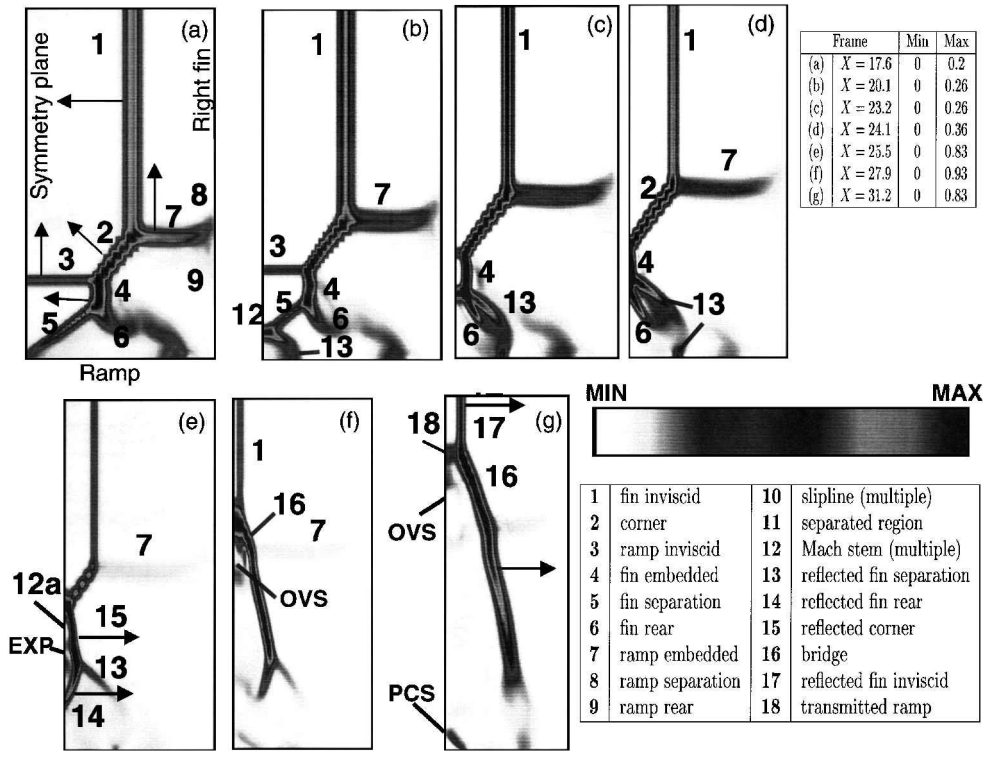

Frame		Min	Max
(a)	X = 17.6	0	0.2
(b)	X = 20.1	0	0.26
(c)	X = 23.2	0	0.26
(d)	X = 24.1	0	0.36
(e)	X = 25.5	0	0.83
(f)	X = 27.9	0	0.93
(g)	X = 31.2	0	0.83

1	fin inviscid	10	slipline (multiple)
2	corner	11	separated region
3	ramp inviscid	12	Mach stem (multiple)
4	fin embedded	13	reflected fin separation
5	fin separation	14	reflected fin rear
6	fin rear	15	reflected corner
7	ramp embedded	16	bridge
8	ramp separation	17	reflected fin inviscid
9	ramp rear	18	transmitted ramp

Fig. 2 Magnitude of pressure gradient at various cross sections: EXP = expansion, OVS = outer vortical structure, and PCS = plate-centerline shock.

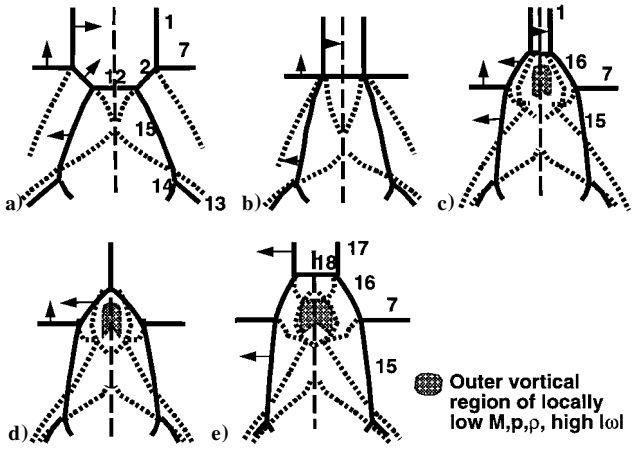

Fig. 4 Schematic representation of reflection of outer shock structure from symmetry plane. Not to scale.

The reflection of the corner shock 2 is relatively rapid and, as noted earlier, irregular. In Fig. 2f, the situation is depicted just before the reflection of the inviscid shock from the symmetry plane. The reflection of the corner shock is complete though the Mach stem (which may be associated with the transmitted ramp shock 18 introduced later) persists. In the final frame, Fig. 2g, the inviscid shock has also reflected off the symmetry plane. A plate centerline shock structure (PCS), which exists but is not so prominent in earlier frames, is also marked. This arises from an impingement of wall-jet-like features as described in Ref. 3.

The sequence of events between Figs. 2e and 2g is also intricate and is sketched in Fig. 4. Figure 4a depicts the features just before the termination of the corner shock 2. The reflection of the corner shock is complete in Fig. 4b. The inviscid shock approaches the symmetry plane in Fig. 4c, which is a schematic of Fig. 2f. A bridge shock 16 is formed, joining the fin inviscid, 1, and ramp embedded, 7, shocks. Slip lines emanate from each of the triple points, 1-12-16 and 7-15-16, as shown in Fig. 4d, where 1 reflects off the symmetry plane. The slip lines form a compact vortical region near the centerline characterized by locally low Mach number, density, and static pressure and high vorticity. The interior of this structure is difficult to discern with the present algorithm and is not detailed. However, the feature appears to be inviscid in origin because independent calculations with the Euler equations (not described here) also show similar development. In Fig. 4e, the inviscid shock has reflected off the symmetry plane to form 17: this situation is shown in Fig. 2f. A transmitted ramp shock, 18, is formed, whose effect is to account for the ramp deflection in the far downstream regions. In the experiment, this has been noted as a Mach stem. The ramp transmitted shock moves upward more rapidly than the ramp embedded shock 7. This follows from the fact that 7 deflects fluid that has previously been processed through 1 alone, whereas 18 processes the relatively lower Mach number fluid downstream of 1 as well as its reflection 17.

III. Conclusions

Computations have been utilized to investigate the shock structure in the multiple-shock/turbulent-boundary-layer interaction comprised by the triple-shock geometry. Near the ramp surface, there is significant similarity to symmetric DF interactions whose shock structure can be described in terms of the reflection of a λ shock from the symmetry plane. For this reason, near the surface, a commonality exists in the DF and TS flowfields in the principal coherent streamline features as has been shown in Ref. 4. The TS outer shock structure is, however, vastly more intricate. The various shock and slip surface components are augmented by an outer vortical structure, all of which are detailed with schematic interpretations.

Acknowledgments

This work was supported by the Air Force Office of Scientific Research sponsorship of Len Sakell and by a grant of computer time from the Department of Defense High Performance Computing Shared Resource Center, Corps of Engineers Waterways Experiment Station, Vicksburg, Mississippi.

References

[1]Garrison, T. J., Settles, G. S., and Horstman, C. C., "Measurements of the Triple Shock/Wave Turbulent Boundary-Layer Interaction," *AIAA Journal*, Vol. 34, No. 1, 1996, pp. 57–64.

[2]West, J. E., and Korkegi, R. H., "Supersonic Interaction in the Corner of Intersecting Wedges at High Reynolds Number," *AIAA Journal*, Vol. 10, No. 5, 1972, pp. 652–656.

[3]Gaitonde, D., and Shang, J. S., "The Structure of a Double-Fin Turbulent Interaction at Mach 4," *AIAA Journal*, Vol. 33, No. 12, 1995, pp. 2250–2258.

[4]Gaitonde, D. V., and Shang, J. S., "On 3-D Shock-Wave Turbulent Boundary Layer Interactions at Mach 4," AIAA Paper 96-0043, Jan. 1996.

A. D. Belegundu
Associate Editor

Fatigue Analysis of Cracked Aluminum Plates Repaired with Bonded Composite Patches

T. Y. Kam,* Y. C. Tsai,† K. H. Chu,† and J. H. Wu†
National Chiao Tung University,
Hsin Chu 300, Taiwan, Republic of China

I. Introduction

BONDED repair of aging structures with composite patches has been an important subject of research in recent years. Investigators have proposed various numerical techniques for stress analysis of repaired structures and the subsequent derivation of stress intensity factors.[1–10] A number of researchers have studied the fatigue behavior of cracked structures repaired with bonded composite patches.[11–13] For instance, Baker[12] studied the fatigue crack propagation of centrally cracked aluminum panels patched with boron/epoxy composites, and Leibovich et al.[13] investigated the effect of composite patches on the fatigue crack growth behavior of repaired parts. In previous work on fatigue behavior of repaired parts, effort has been devoted to the fatigue of repaired parts with center cracks. Though edge cracks developed in thin-wall type structural members are not uncommon, as yet not much work has been done in the fatigue of bonded repair of parts with edge cracks. In this Note, fatigue behavior of aluminum panels containing an edge crack repaired with bonded composite patches is studied. A method is proposed for determining stress intensity factor and fatigue life of the repaired structures. Strain at the crack tip obtained in the finite element analysis of the repaired structure is used to determine the stress intensity factor of the structure. The Paris law of crack propagation is used to predict fatigue life of the repaired structure. Fatigue tests of compact tension (C–T) specimens with and without bonded repairs under different environmental conditions are performed to validate the accuracy and feasibility of the proposed method.

II. Analytical Approach

Finite Element Model

The aluminum plate with an edge crack (Fig. 1) is symmetrically repaired with bonded composite patches. The patches are modeled as Mindlin plates and analyzed using eight-noded serendipity elements. The adhesive and the aluminum plate are modeled by three-dimensional brick elements of 20 nodes. The aspect ratio of the three-dimensional brick elements are chosen in such a way that no numerical instability will occur. Quarter-point elements are used to model the stress singularity condition at the crack tip. The compatibility conditions at the interfaces between the patch, adhesive, and cracked plate are observed in the finite element formulation. When studying crack propagation, perfect bonding at the interfaces

Received Sept. 30, 1996; revision received Sept. 6, 1997; accepted for publication Sept. 26, 1997.

*Professor, Department of Mechanical Engineering. Member AIAA.
†Graduate Student, Department of Mechanical Engineering.